Dielectron measurements with the HADES at GSI

Jan-Hendrik Otto[1] for the HADES collaboration
e-mail: jan.h.otto@physik.uni-giessen.de

[1]Justus-Liebig University Giessen

Abstract. In this work we present the dielectron analysis of 4.5 billion Ag+Ag collisions ((0−40)% centrality) at a center-of-mass energy of $\sqrt{s_{NN}} = 2.55\,GeV$ measured with HADES. The obtained dielectron signal spectrum is compared to simulated hadronic cocktail and nucleon-nucleon reference spectra revealing a strong contribution from the hot and dense phases. The average temperature of the collision system can be extracted from the slope of the in-medium contribution. In a momentum differential analysis we observe modifications of the dielectron signal shape in the $\omega-\rho$ invariant mass region. Furthermore we compare the results to previous measurements in Au+Au collisions at slightly lower energy. The suggested modifications of the ρ spectral function is further studied within the HADES pion-beam program. Here, we present recently published results on the electromagnetic and hadronic coupling of baryonic resonances to the $\rho - N$ final state.

1 Introduction

The **H**igh **A**cceptance **DiE**lectron **S**pectrometer (HADES) [1] is dedicated to the measurement of electromagnetic and rare hadronic [2] probes from elementary to heavy-ion collisions and the study of the in-medium behaviour of dileptons, as their spectral distributions reveal the thermal properties of the medium. In heavy-ion collisions at $\sqrt{s_{NN}} = 2 - 3\,GeV$ as measured with HADES, matter is compressed to 2-3 times the ground-state density and heated up to temperatures of about $T = 70\,MeV$ [3], thus HADES is investigating the moderate temperature and high-density region of the QCD phase diagram. In order to study the electromagnetic and hadronic couplings of baryonic resonances to the $\rho - N$ final state, which is particularly important for the understanding of the emissivity of hot and dense nuclear matter due to the important role of intermediary vector mesons in dilepton emission, HADES has initiated a dedicated pion-nucleon program [4]. Baryon-meson couplings and the validity of the vector dominance model for baryon transitions were investigated in the second resonance region, the importance of the latter clearly being underlined [5].

2 The HADES experiment

HADES is a fixed target experiment located at the SIS 18 accelerator at GSI, Germany. It is constructed as a magnet spectrometer covering nearly the full forward hemisphere apart from small polar angles. Four layers of low mass **M**ini-**D**rift-**C**hambers (MDCs) located in front (2) and behind (2) the magnetic field region provide tracking information. Time of

flight measurement is performed by **R**esistive **P**late **C**hambers (RPCs) and a ToF wall at polar angles of 18° − 44° and 44° − 88°, respectively. A hadron blind **R**ing **I**maging **CH**erenkov detector (RICH) considerably enhances electron identification. Recently, the RICH detector has been upgraded with a new photon detector consisting of 428 64-channel H12700 ***Multi-Anode PMTs*** (MAPMTs) with FPGA based readout [6]. Furthermore an electromagnetic calorimeter has been added. In the presented Ag+Ag data it covered only a small fraction of the total HADES acceptance.

3 Ag+Ag collisions at $\sqrt{s_{NN}} = 2.55\,\mathrm{GeV}$

3.1 Detector performance - Electron identification

Electron identification is performed by matching reconstructed tracks to rings in the hadron blind RICH detector and using time-of-flight information. Misidentification of mainly pions arises from random matching of pion tracks to RICH rings. Simulation studies using UrQMD [7] however suggest an electron purity of $P > 99\,\%$ at low and $P \approx 90\,\%$ at high momentum, compare fig. 1, left, for momentum integrated data. Accordingly, a pion suppression in the order of 10^5 is achieved. These values match to the purely data based RICH rotation technique, giving a measure for random ring-to-track matching. The purity of the electron sample will be even further improved with a fully equipped and properly calibrated electromagnetic calorimeter in future.

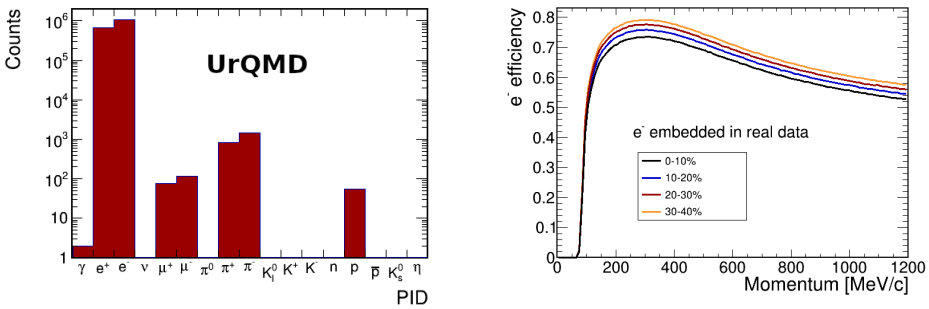

Figure 1. Left: Particle abundances in UrQMD simulations (90 million collisions) after applying the electron selection criteria used in data. Right: Electron efficiency as a function of momentum and centrality (track density) obtained from simulated electron tracks embedded into real data.

The single electron efficiency is calculated by embedding simulated electrons into real data. It exceeds $\epsilon > 0.5$ over the whole momentum range and reaches up to $\epsilon \sim 0.75$ at small momenta, compare fig. 1, right. With increasing track density, i.e. centrality of the events, the tracking efficiency is reduced resulting in a slight centrality dependence of the single electron efficiency.

The upgraded RICH detector does not only combine high electron efficiency and pion suppression, but also provides the possibility to identify conversion electrons. In most conversion processes, only one electron can be tracked, enhancing the combinatorial background. Ring finding based on Hough-Transformation [8] can separate rings with opening angles larger than $\alpha \sim 2°$ (fig. 2, middle), significantly exceeding the double-track separation of the MDCs and not being affected by acceptance losses at small momenta due to the magnetic field. The

observation of close-by rings ($\alpha < 9°$) is thus used to identify conversion processes. Furthermore, the identification of conversion processes down to opening angles $\alpha \to 0°$ is possible due to the amount of Cherenkov photons in the vicinity of a reconstructed ring, which is roughly twice the amount for conversion processes as for single electrons (compare fig. 2, left and right). With an average amount of $N_\gamma = 16$ a distinction between one and two electron signals is well possible.

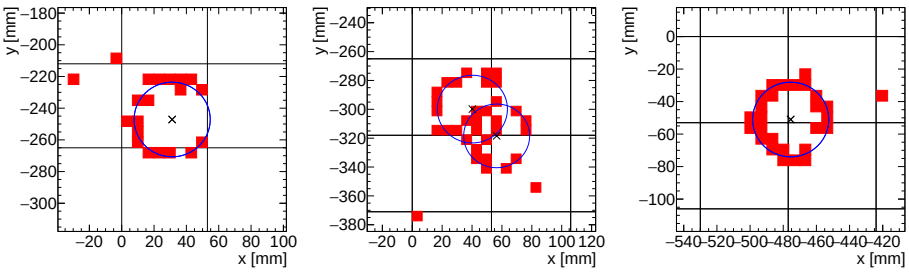

Figure 2. Reconstructed rings from detected Cherenkov photons on the HADES RICH MAPMT plane; zoom-in views of single event displays. Left: Signature of one electron. Center: Two rings from an electron pair with an opening angle $\alpha \sim 2°$. Right: Only one ring can be reconstructed for pair opening angles $\alpha \to 0°$.

3.2 Pair invariant mass distribution

Dielectrons are formed pairing each reconstructed electron with each positron in a collision (compare fig. 3). Single lepton momenta are restricted to $0.1\,GeV/c < p < 1.2\,GeV/c$ and the pair opening angle is required to exceed $\alpha > 9°$. The combinatorial background arising in the pairing of electrons and positrons can be described by the geometrical mean of same-event e^+e^+ and e^-e^- pairs ($\langle FG_{++}\rangle, \langle FG_{--}\rangle$) weighted with the so called *k-factor*. This accounts

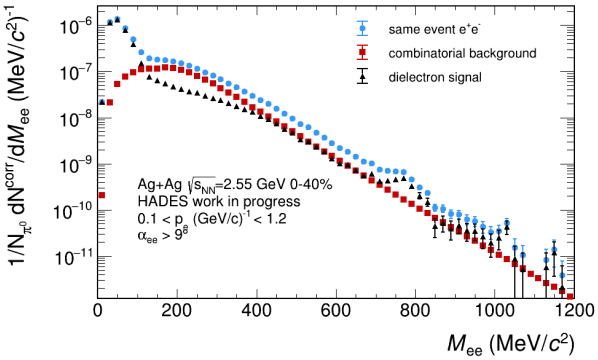

Figure 3. Efficiency corrected invariant mass distribution of reconstructed dielectrons in the HADES acceptance. Subtracting the combinatorial background (see *text* for the calculation details) from the same-event data yields the signal data.

for acceptance and reconstruction differences in the pairings and is derived using the event-mixing technique, see formula 1 [9].

$$\langle BG_{+-}\rangle = k \cdot 2\sqrt{\langle FG_{++}\rangle\langle FG_{--}\rangle} \quad with \quad k = \frac{\langle fg_{+-}\rangle}{2\sqrt{\langle fg_{++}\rangle\langle fg_{--}\rangle}} \tag{1}$$

Within the event-mixing, electrons and positrons reconstructed in different events are paired ($\langle fg_{+-}\rangle$, $\langle fg_{++}\rangle$,$\langle fg_{--}\rangle$), which allows for almost unlimited statistics. The same-event like-sign combinatorial background evaluation is used for low invariant masses $M_{ee} < 300\,MeV/c^2$. For larger masses the background is obtained from mixed events only in order to reduce statistical errors. Normalization to the same event background is obtained in the region $300\,MeV/c^2 < M_{ee} \leq 700\,MeV/c^2$. The derived combinatorial background distribution and the dielectron signal in the HADES acceptance are shown in fig. 3. A centrality dependent efficiency correction based on single tracks, derived by embedding simulated electrons into real data (compare fig. 1, right), is applied.
In the $\rho - \omega$ mass region a clear enhancement above the exponential slope is visible and pairs up to the ϕ-meson pole mass are reconstructed. The signal-to-background ratio surpasses unity for $M_{ee} > 500\,MeV/c^2$ and reaches up to 3 at around the ω-meson pole mass. This analysis excluding the conversion rejection based on the RICH reduces the signal-to-background ratio by almost one order of magnitude compared to an analysis not using this information, clearly pointing out the huge gain in precision achieved within the RICH upgrade.

3.3 Extraction of the in-medium contribution

The signal extracted in fig. 3 is composed of the dielectrons produced within the whole evolution of the colliding system. In order to access the hot and dense phase, all known contributions are simulated and subtracted. Using the transport model GiBUU [11], $p + p$ and $p + n$ collisions are simulated to estimate the contribution of initial NN collisions. The weighting is performed via $NN = 0.54\,pp + 0.46\,pn$ [3]. The relevant channels taken into account are bremsstrahlung processes and $\Delta \rightarrow Ne^+e^-$. Dielectron production through the decay of freeze-out hadrons is addressed performing PLUTO [10] simulations of the relevant

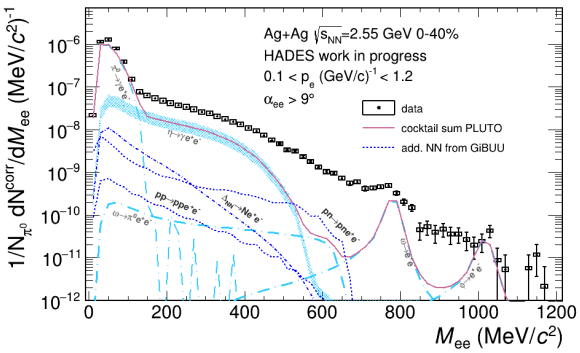

Figure 4. Decomposition of the measured dielectron signal (compare fig. 3) into its contributions from the different stages of the heavy-ion collision. PLUTO [10] simulations are used to address the freeze-out hadron contribution while the transport model GiBUU [11] is used to model dielectron production in the initial NN collisions.

hadrons ($\pi^0, \eta, \omega, \phi$) with subsequent embedding into UrQMD simulations and analysis as for real data. The hadron multiplicities required for scaling the simulated spectra are estimated within the same data sample: The π^0- and $\eta-$mesons are reconstructed via their $4e$ decay pattern, the ω is analyzed via $\omega \rightarrow e^+e^-$ and the Φ in its decay into two kaons. In case of the η, the work-in-progress multiplicity contains a systematic error of about 30 %, which is in the following visualized as a band in the corresponding spectra. The dielectron signal together with the simulated initial NN contribution and the hadronic cocktail is shown in fig. 4. Over the full invariant mass range, a strong excess in dielectron production beyond the simulated sources is observed, which we refer to as in-medium radiation. This dielectron radiation from the hot and dense phases still including contributions from the $\rho-$meson is addressed by subtracting the simulated sources from the total dielectron yield and is further studied in order reveal the thermal properties of the medium. Fig. 5 shows the in-medium radiation after performing an acceptance correction to 4π. It follows an exponential shape indicating thermal production. Thus, the data can be described using $dN/dM_{ee} \propto M_{ee}^{3/2} exp(-M_{ee}/kT)$ as fit function, where the inverse slope of the spectrum corresponds to an average temperature of the medium. The fit reveals $kT = 77.9^{+3.7}_{-3.0}\, MeV$ with the combined error dominated by the uncertainty in the η multiplicity, indicated by a yellow band. As expected, the value is slightly larger compared to the temperature measured in Au+Au collisions by HADES at $\sqrt{s_{NN}} = 2.42\, GeV$ [3].

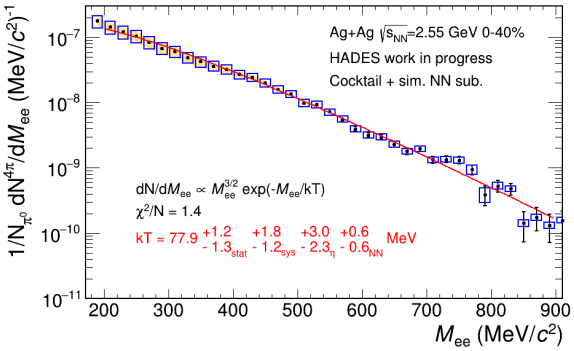

Figure 5. Subtraction of the hadronic cocktail and the initial NN contribution reveals the in-medium dielectron signal. The exponential shape is fitted with a thermal distribution resulting in an integrated medium temperature of $T \sim 78\, MeV$. The uncertainty in the η multiplicity is indicated by the yellow band.

3.4 Pair momentum differential analysis

In a next step, the dielectron data is analyzed in the same way as previously presented, but in three bins of transverse pair momentum in order to tentatively select pairs moving with or faster than the fireball. We introduce a low momentum bin with transverse pair momenta $p_t < 0.4\, GeV/c$, a medium momentum bin, $0.4\, GeV/c < p_t < 0.7\, GeV/c$, and a high momentum bin with $0.7\, GeV/c < p_t$. The dielectron signal in all three bin is presented in fig. 6. The thermal continuum is fitted in each bin in the invariant mass region $200\, MeV/c^2 < M_{ee} < 500\, MeV/c^2$ shown as a dashed line ($dN/dM_{ee} \propto M_{ee}^{3/2} exp(-M_{ee}/kT)$). In the low momentum bin, we observe a broad enhancement in the $\rho-\omega$ invariant mass region above the continuum,

which transforms into a peak structure with increasing transverse pair momentum. These modifications in the line-shape indicate strong in-medium modifications, not only of the ρ meson but also of the ω. However, in order to perform a detailed analysis of the ω line-shape (in bins of pair momentum), theory calculations of the ρ line-shape need to be taken as input. Corresponding calculations are currently performed. In the high momentum bin we observe a second peak structure located at around $M_{ee} \sim 550\, MeV/c^2$. The origin of this unexpected structure is currently investigated.

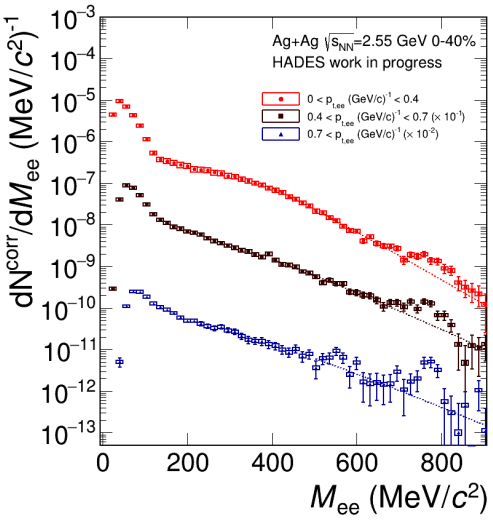

Figure 6. Dielectron signal in bins of the transverse pair momentum. With increasing momentum, significant modifications in the line-shape are observed. The dashed line is a fit to the thermal continuum ($dN/dM_{ee} \propto M_{ee}^{3/2} exp(-M_{ee}/kT)$).

4 Au+Au collisions at $\sqrt{s_{NN}} = 2.42\,\mathbf{GeV}$

Within the HADES heavy-ion program, also Au+Au collisions at $\sqrt{s_{NN}} = 2.42\, GeV$ have been measured. The analysis [3] has been carried out similarly as in the presented Ag+Ag data, however the data was taken before the RICH upgrade yielding a signal-to-background ratio of $S/B_{Au+Au} \sim 0.15$ instead of $S/B_{Ag+Ag} \sim 1$. Elementary NN collisions have been studied by HADES at the same energy [12], allowing for a straight forward extraction of the in-medium contribution. Besides the NN data, simulated contributions from the η and ω have to be additionally subtracted accounting for sub-threshold production in A+A collisions. The remaining in-medium contribution is shown in fig. 7 together with various model calculations. The spectrum appears very similar as in the Ag+Ag data, being characterized by a structure-less, near exponential shape. A description with the thermal function yields an average medium temperature of $kT = 71.8 \pm 2.1\, MeV$ being slightly lower as in Ag+Ag and thus in agreement regarding the lower beam energy. A strong medium modification of the ρ spectral function in the model calculations is required in order to reproduce the data. The usage of a vacuum ρ spectral function clearly underestimates the dielectron yield towards

lower invariant masses and would create a shoulder structure at around the nominal pole mass which is not observed.

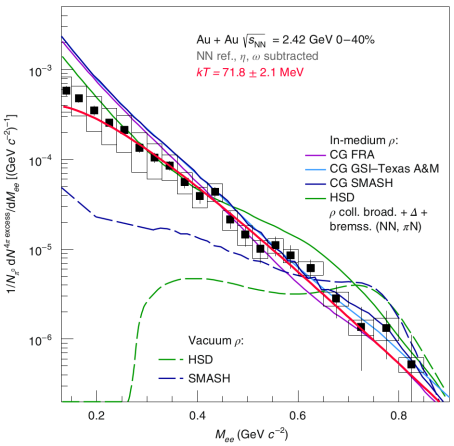

Figure 7. In-medium dielectron spectrum in Au+Au collisions at $\sqrt{s_{NN}} = 2.42\,GeV$ measured by HADES in comparison with calculations for the ρ line-shape [3].

5 $\pi^- + CH_2$ at $\sqrt{s_{\pi^- p}} = 1.49\,GeV$

In order to further study the strong in-medium modification of the $\rho-$meson observed in the heavy-ion data which is potentially caused by strong coupling to baryonic resonance states,

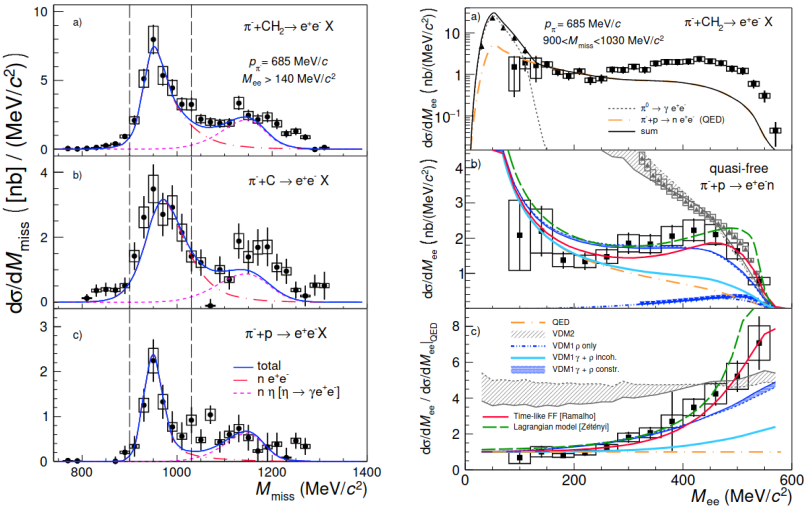

Figure 8. Left: Efficiency corrected missing mass distribution in the $\pi^- p$ system for a fixed pion-beam momentum of $p = 0.695\,GeV/c$. Vertical lines indicate the missing mass window used to select the $\pi^- p \to ne^+e^-$ channel. Right: $d\sigma/dM_{ee}$ in the specified missing mass range. Data after subtraction of the π^0 Dalitz contribution is shown in comparison to model calculations in (b) and (c). [5]

HADES has initiated a dedicated pion beam program. The setup allows for a resolution of 0.1% to 0.3% in pion-beam momentum in order to study reactions of the type $\pi+N \rightarrow Ne^+e^-$ in the second resonance region [4]. HADES measured the dielectron production in $\pi^- + CH_2$ and $\pi^- + C$ collisions in order to extract $\pi^- + p$ data by combining both measurements. The missing mass distributions in the $\pi^- + p \rightarrow Xe^+e^-$ is shown in fig. 8 (left). A missing mass requirement around the neutron mass allows a selection of $\pi^- + p \rightarrow ne^+e^-$ reactions, allowing for the first ever cross-section measurement in this energy region yielding $\sigma = (2.97 \pm 0.38)\,\mu b$ [5], providing necessary input for theory. A comparison of the invariant mass distribution with various model calculations allows to investigate the validity of the vector dominance model for baryon transitions, which is elaborated in detail in [5].

6 Summary

We have presented new dielectron spectra of the HADES collaboration for Ag+Ag collisions at $\sqrt{s_{NN}} = 2.55\,GeV$ showing an unprecedented quality in terms of statistics and S/B ratio. The upgraded RICH detector combines high efficient electron detection with impressive pion and γ conversion recognition. The integrated medium temperature is estimated from the extracted in-medium contribution to $kT = 77.9^{+3.7}_{-3.0}\,MeV$. A pair momentum differential analysis shows a modification of the dielectron signal in the $\rho - \omega$ invariant mass region. HADES has observed a structure-less, near exponential shaped in-medium contribution also in the earlier studied Au+Au collisions suggesting a strong in-medium modification of the ρ meson. A dedicated pion beam program has been initiated by HADES to further study the coupling of the ρ meson to baryonic resonance states which might cause the observed modifications in hot and dense matter.

References

[1] G. Agakishiev et al. (HADES), Eur. Phys. J. A **41**, 243 (2009), 0902.3478
[2] J. Adamczewski-Musch et al. (HADES), Phys. Lett. B **778**, 403 (2018), 1703.08418
[3] G. Agakishiev et al. (HADES), Nature Physics **15**, 1040 (2019)
[4] P. Salabura, J. Stroth, L. Fabbietti (HADES), Nucl. Phys. News **25**, 22 (2015)
[5] R. Abou Yassine et al. (HADES) (2022), 2205.15914
[6] C. Pauly et al., Nuclear Instruments and Methods in Physics Research Section A: Accelerators, Spectrometers, Detectors and Associated Equipment **876**, 164 (2017), the 9th international workshop on Ring Imaging Cherenkov Detectors (RICH2016)
[7] S.A. Bass et al., Prog. Part. Nucl. Phys. **41**, 255 (1998), nucl-th/9803035
[8] S.A. Lebedev, G.A. Ososkov, Phys. Part. Nucl. Lett. **6**, 161 (2009)
[9] A. Adare et al. (PHENIX Collaboration), Phys. Rev. C **81**, 034911 (2010)
[10] I. Fröhlich et al., PoS **ACAT**, 076 (2007), 0708.2382
[11] O. Buss, T. Gaitanos, K. Gallmeister, H. van Hees, M. Kaskulov, O. Lalakulich, A.B. Larionov, T. Leitner, J. Weil, U. Mosel, Phys. Rept. **512**, 1 (2012), 1106.1344
[12] G. Agakishiev et al. (HADES), Phys. Lett. B **690**, 118 (2010), 0910.5875